Structural Chemistry
https://doi.org/10.1007/s11224-023-02226-9

RESEARCH

Computational study on alkali and alkaline earth metal decorated B_{20} cluster for hydrogen storage application

Parimala devi Duraisamy[1] · Prince Makarios Paul S[1] · Praveena Gopalan[2] · Abiram Angamuthu[1]

Received: 24 June 2023 / Accepted: 30 August 2023

Abstract

The potential of B_{20} cluster decorated with alkali metals (AM = Li, Na, and K) and alkaline earth metals (AEM = Ca, Mg, and Be) to adsorb hydrogen molecules is investigated using density functional theory (DFT). The Bader's topological parameters suggest the presence of non-bonded interaction between the bare structures and H_2 molecules. Global reactivity descriptor values confirm that the structures remain stable even after the adsorption of H_2 molecules. The results indicate that Na adorned B_{20} ($B_{20}Na_2$) can store up to $12H_2$ molecules, with a hydrogen storage capacity of 8.33 wt% and an average adsorption energy is 0.127 eV/H_2. The findings suggest that B_{20} cluster decorated with AM and AEM have the ability to be a promising hydrogen storage material. Additionally, to gain insights into the adsorption and desorption behaviors of H_2 molecules, ADMP molecular dynamics simulations methods were performed at room temperatures.

Keywords Hydrogen storage · DFT · B_{20} cluster · Alkali metals · Alkaline earth metals

Introduction

Nowadays, the growing global population has significantly increased human living standards. Conventional energy sources can no longer meet the demand for energy, which is limited and may pollute the environment if utilized in an excessive manner [1, 2]. Recently, hydrogen is regarded as a promising energy carrier with the potential to replace fossil fuels owing to its vast availability, great efficiency, and environmental friendliness [3, 4]. However, obtaining a viable hydrogen storage technology remains a major challenge in the current decade. As a result, more study into the strategies to accomplish safe and effective hydrogen storage is most required. The US Department of Energy has revised its hydrogen storage capacity for 2025 to a gravimetric density of 5.5 wt% at ambient temperature. Indubitably, developing a cost-effective hydrogen storage system is still a long way off [5]. To solve this problem several materials have been investigated for their potential in hydrogen storage [6, 7]. Mahamiya et al. explored the scandium decorated C_{24} fullerene, which showed the ability to hold up to six H_2 molecules with a gravimetric density of 13.02 wt% [8]. Another study, in the same research group, studied the yttrium-doped C_{24} fullerene, demonstrating a maximum adsorption of $6H_2$ molecules with an average adsorption energy of − 0.37 eV and an average desorption temperature of 477 K [9]. El Kassaoui et al. examined metal decorated beryllium carbide, finding that 2Li@Be_2C and 2 K@Be_2C could host up to $16H_2$ molecules, resulting in gravimetric capacities of 10.21 and 8.48 wt%, respectively [10]. Additionally, the same research group explored the t-graphene-like boron nitride monolayer (t-B_4N_4) for hydrogen storage applications. By replacing carbon atoms in t-graphene with boron and nitrogen atoms, they achieved a Li-decorated double-sided t-B_4N_4 capable of storing up to $32H_2$ molecules. This material exhibited average hydrogen adsorption energy of 0.217 eV per H_2 and a maximum hydrogen storage capacity of 12.47 wt% [11].

In general, hydrogen molecules cannot be adequately adsorbed as their binding to the surface of pristine nanostructures is highly influenced by the Van der Waals interaction [12]. However, metal doping on boron clusters has shown to be a successful and useful technique for enhancing the adsorption capability for H_2 molecules. Henceforth, several metal-decorated nanostructures were studied through experimental and

✉ Abiram Angamuthu
aabiram@gmail.com

[1] Department of Physics, Karunya Institute of Technology and Sciences, Coimbatore, 641114 Tamilnadu, India

[2] Department of Physics, PSGR Krishnammal College for Women, Coimbatore, 641004 Tamilnadu, India

Published online: 11 September 2023

theoretical methods [13–17]. Among those, due to their light weight and distinctive electronic properties, boron nanostructures have recently received significant attention from researchers compared to carbon nanostructures. Boron clusters (B_n, $n > 20$) with metal decorations are commonly suggested as promising hydrogen storage materials [18, 19]. Indeed, metals adorned with smaller boron structures (B_n, $n < 20$) are also found to be effective hydrogen storage compounds [20].

Among alkali (AM = Li, Na, and K) and alkaline earth metals (AEM = Ca, Mg, and Be), decorated boron materials exhibit outstanding hydrogen storage capabilities [17–22]. In the investigation of Na coated B_{36} boron sheets, Ye et al. observed that these clusters had a 4.4 wt% hydrogen storage capacity and could thus accommodate up to $10H_2$ molecules [23]. Alkali metal (AM = Li, Na, and K) doped B_{80} fullerene was studied for its hydrogen storage potential by Yuanchang et al. and higher gravimetric densities were observed for Na- and K-doped fullerene (11.2 wt% and 9.8 wt%) [24]. Mao et al. studied the metal atoms (M = Li, Ca, Sc, and Ti) coated B_{40} clusters and identified that $6Ca@B_{40}$ could hold up to $24H_2$ molecules with an average adsorption energy of 0.170 eV/H_2 which resulted in a gravimetric density of 6.66 wt% [25]. Liu et al. examined the hydrogen storage performance of Ca decorated B_{36}, finding that each Ca atom can hold up to $6H_2$ molecules with preferable adsorption energy of 0.364 eV/H_2, yielding a gravimetric density of 4.97 wt% [26]. Wang et al. reported that the gravimetric density of Ca-decorated novel boron sheet was 12.68 wt% and its average binding energy varied from − 0.20 to − 0.32 eV/H_2 [27].

Recently, boron clusters have aroused the interest of researchers due to the fact that their properties vary depending on size, component, and structure. Kiran et al. studied the neutral and anionic B_{20} clusters using experimental and computational simulations and identified the B_{20} neutral cluster has a double-ring tubular structure with a diameter of 5.2 Å [28]. An et al. investigated the stability of planar versus double-ring tubular isomerism using neutral and anionic B_{20} clusters [29]. Lu et al. extensively investigated the structural and electronic characteristics of C- and Si-doped B_{20} clusters through semi-empirical quantum mechanics method and identified that substitution of C and Si atoms noticeably alters the structural features of B_{20} clusters [30]. Although there have been a several number of theoretical and experimental studies on hydrogen storage applications published in literatures to date, however, there is no study have been published on B_{20} with alkali and alkaline earth metals [31–33]. Therefore, we aim to examine the hydrogen storage capabilities of alkali (Li, Na, and K) and alkaline earth metals (Ca, Mg, and Be) decorated B_{20} boron cluster based on density functional theory (DFT) calculations. The obtained results may contribute to the development of B_{20}-based nanostructures for hydrogen storage applications.

Computational details

DFT calculations were employed to examine the stability, electronic, and storage properties of H_2 molecules on alkali (Li, Na, and K) and alkaline earth metals (Ca, Mg, and Be) decorated B_{20} at the ωB97XD/6–311 + + G(d,p) level of theory [34, 35]. At the same theoretical level, the natural bonding orbitals (NBO) were calculated. The nature of the interaction between bare cluster and hydrogen molecules was investigated using quantum theory of atoms in molecule (QTAIM) with the aid of Multiwfn software [36]. Analyzing their global reactivity descriptors, such as hardness (η), electrophilicity (ω), and electronegativity (χ) led to better understanding of the stability and reactivity of alkali- and alkaline earth metals–decorated boron clusters and their H_2 interacted systems. Additionally, the energy gaps (E_g) between the highest occupied molecular orbitals (HOMOs) and lowest unoccupied molecular orbitals (LUMOs) of the clusters are calculated in order to determine their kinetic stabilities [37]. The following expressions represent the hardness (η), electronegativity (χ), and electrophilicity (ω).

$$\eta = \frac{1}{2}\left(E_{\mathrm{LUMO}} - E_{\mathrm{HOMO}}\right) \tag{1}$$

$$\chi = -\frac{1}{2}\left(E_{\mathrm{LUMO}} + E_{\mathrm{HOMO}}\right) \tag{2}$$

$$\omega = \frac{\mu^2}{2\eta} \tag{3}$$

Presently, the following expression can be used to evaluate the gravimetric density (wt%) for hydrogen storage.

$$\mathrm{H_2(wt \cdot \%)} = \left[\frac{M_{H_2}}{M_{H_{2+}M_{Host}}}\right] \times 100 \tag{4}$$

Where M_{H_2} and M_{Host} are mass of maximum hydrogen molecules adsorbed over the system and mass of the host structure, respectively. All the simulation studies were executed in Gaussian 09W software [38], and structures are visualized using the Chemcraft software [39].

Results and discussion

The geometry of $B_{20}AM_2$ and $B_{20}AEM_2$ (AM = Li, Na, and K; AEM = Ca, Mg, and Be) clusters

In this section, we first employ the ωB97XD/6–311 + + G(d,p) approach to optimize the planar B_{20} finite cluster. After optimization of bare boron cluster, we have adorned alkali (AM = Li,

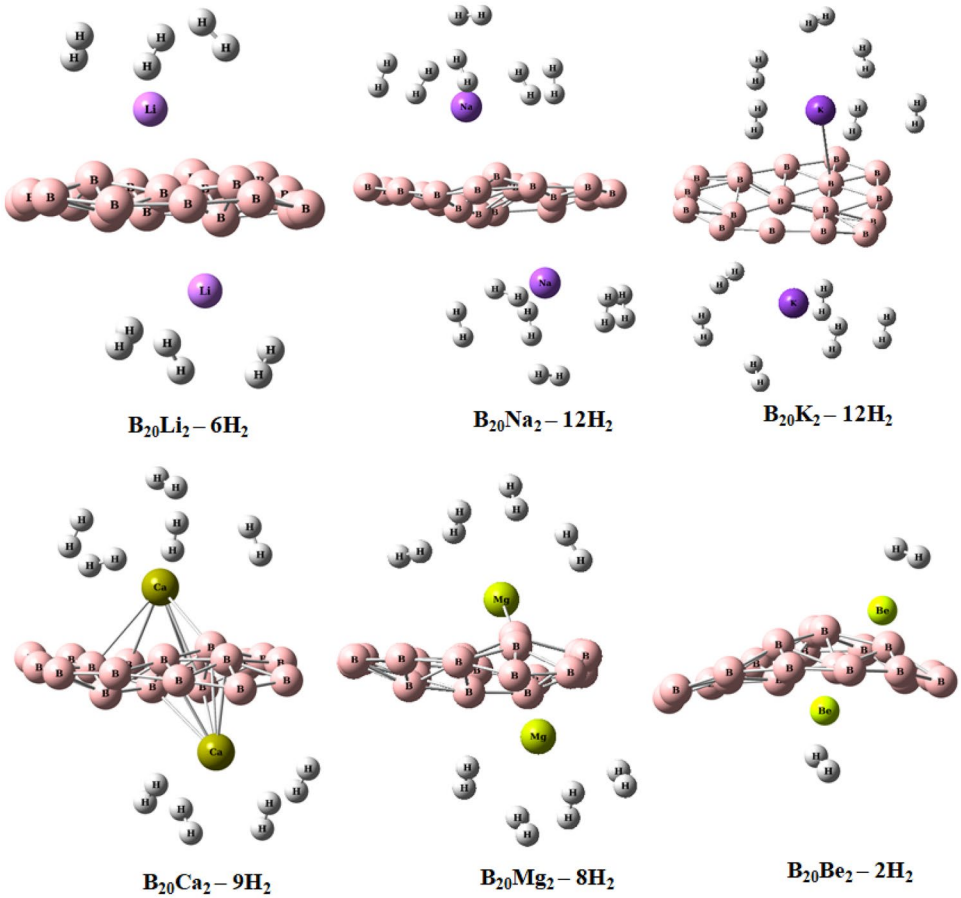

Fig. 1 Optimized geometries of H_2 adsorbed $B_{20}AM_2$ (AM = Li, Na, and K) and $B_{20}AEM_2$ (AEM = Ca, Mg, and Be) complexes

Na, and K) and alkaline earth metals (AEM = Ca, Mg, and Be) on both top and bottom of the boron cluster in the ground state. The bond lengths of boron to lithium (B_{20}-Li_2), sodium (B_{20}-Na_2), and potassium (B_{20}-K_2) are observed to be 2.286 Å, 2.920 Å, and 3.046 Å, respectively, for alkali metal–decorated B_{20} complexes. Similarly, for alkaline earth metal–decorated B_{20} cluster, the bond length of calcium (B_{20}-Ca_2), magnesium (B_{20}-Mg_2), and beryllium (B_{20}-Be_2) are observed to be 2.681 Å, 2.297 Å, and 1.982 Å, respectively. Firstly, one H_2 molecule is added to each Li atom in the $B_{20}Li_2$ structure and it is placed parallel to the boron cluster. After gradually expanding the $B_{20}Li_2$ structure with the addition of H_2 molecules, it was found that it could accommodate up to $6H_2$ molecules and has a quasi-perpendicular arrangement. Similarly for structures $B_{20}Na_2$, $B_{20}K_2$, $B_{20}Ca_2$, $B_{20}Mg_2$, and $B_{20}Be_2$, each structure can hold up to $12H_2$, $12H_2$, $9H_2$, $8H_2$, and $2H_2$ molecules, respectively.

Figure 1 depicts the H_2 adsorption on $B_{20}AM_2$ and $B_{20}AEM_2$ structures, and Table 1 lists the notable average bond lengths for both bare and H_2 adsorbed structures. A nominal change from the bare boron cluster is observed signifying the adsorption of H_2 molecules. The H–H bond distance of the entire complex is not considerably altered and they fall in the range of 0.748 to 0.777 Å when compared to its isolates (0.750 Å). In alkali (B-AM; AM = Li, Na, and K) and alkaline earth metals (B-AEM; AEM = Ca, Mg, and Be) interacted complexes, the B-AM /B-AEM bonds are increased by 0.002–0.232 Å, and this demonstrates that the presence of H_2 molecules does not affect the structural integrity of $B_{20}AM_2$ and $B_{20}AEM_2$ structures. The AM-H/AEM-H bond lengths are found to be in the range of 1.623–2.996 Å in H_2 adsorbed alkali and alkaline earth metal complexes, respectively.

Table 1 Average bond lengths of B-B, B-M (M = Li, Na, K, Ca, Mg, and Be), M-M, M-H, and H–H of the cluster calculated at ωB97XD/6–311 + + G(d,p) level of theory

Complexes	B-B (Å)	B-M (Å)	M-M (Å)	M-H (Å)	H–H (Å)
$B_{20}Li_2$	1.678	2.286	4.047	-	-
$B_{20}Li_2$–$6H_2$	1.675	2.518	4.124	2.223	0.750
$B_{20}Na_2$	1.681	2.920	5.444	-	-
$B_{20}Na_2$–$12H_2$	1.676	2.993	5.527	2.635	0.749
$B_{20}K_2$	1.677	3.046	6.130	-	-
$B_{20}K_2$–$12H_2$	1.673	3.134	6.111	2.996	0.748
$B_{20}Ca_2$	1.690	2.681	4.926	-	-
$B_{20}Ca_2$–$9H_2$	1.687	2.683	4.972	2.586	0.753
$B_{20}Mg_2$	1.704	2.297	4.559	-	-
$B_{20}Mg_2$–$8H_2$	1.666	2.352	4.538	2.553	0.752
$B_{20}Be_2$	1.689	1.982	2.889	-	-
$B_{20}Be_2$–$2H_2$	1.699	1.989	3.107	1.623	0.777

Table 2 The calculated values of HOMO, LUMO and HOMO–LUMO energy gap (E_g), hardness (η), electrophilicity index (ω), and electronegativity (χ) of the structures

Complexes	HOMO (eV)	LUMO (eV)	E_g (eV)	η (eV)	ω (eV)	χ (eV)
$B_{20}Li_2$	−7.213	−2.156	5.057	2.529	4.340	4.685
$B_{20}Li_2$–$6H_2$	−7.038	−2.036	5.002	2.501	4.115	4.537
$B_{20}Na_2$	−7.141	−1.769	5.372	2.686	3.695	4.455
$B_{20}Na_2$–$12H_2$	−6.769	−1.586	5.183	2.592	3.367	4.178
$B_{20}K_2$	−6.601	−1.451	5.150	2.575	3.147	4.026
$B_{20}K_2$–$12H_2$	−6.443	−1.457	4.986	2.493	3.129	3.950
$B_{20}Ca_2$	−6.152	−1.496	4.656	2.328	3.141	3.824
$B_{20}Ca_2$–$9H_2$	−6.018	−1.222	4.796	2.398	2.732	3.620
$B_{20}Mg_2$	−6.648	−1.793	4.855	2.428	3.669	4.221
$B_{20}Mg_2$–$8H_2$	−6.271	−1.362	4.909	2.455	2.967	3.817
$B_{20}Be_2$	−7.066	−2.362	4.704	2.352	4.724	4.714
$B_{20}Be_2$–$2H_2$	−7.128	−2.362	4.766	2.383	4.724	4.745

HOMO–LUMO analysis

To better comprehend the electronic properties upon H_2 adsorption, calculations on frontier molecular orbitals (FMOs) are performed. The energies of HOMO, LUMO, energy gap (E_g), hardness (η), electrophilicity (ω), and electronegativity (χ) of the structures are calculated at ωB97XD/6–311 + + G(D,P) level of theory and the values are listed in Table 2. The findings demonstrate that the complexes exhibit an increase in values of hardness with decrease in electrophilicity. However, in contrast, for alkali metal complexes the values of hardness decrease when compared to its isolates. Among, $B_{20}Na_2$–$12H_2$ has the highest η (2.592 eV), $B_{20}Ca_2$ –$9H_2$ has the lowest ω (2.732 eV), and maximum ω (4.724 eV) is observed for $B_{20}Be_2$–$2H_2$ complexes. Additionally, we observed that χ values decreased after adsorption of H_2 molecules in $B_{20}AM_2$ and $B_{20}AEM_2$ structures. The highest value of χ was identified for $B_{20}Be_2$ (4.745 eV) and the lowest for $B_{20}Ca_2$ (3.620 eV) complexes. Hence, minimum electrophilicity and maximum hardness principles ensure that the stability of complex is enhanced after successive adsorption of hydrogen molecules. Furthermore, it was observed that the values of electronegativity (χ) decrease with the addition of H_2 molecules, showing that the complexes are less likely to lose electrons, therefore implying the enhanced stability of the considered complexes. Moreover, the calculated energy gap (E_g) values gradually increased upon addition of the hydrogen molecule adsorption for alkaline earth metal–decorated complexes. However, a reverse trend is observed for alkali metal–adorned complexes.

Natural bond orbital (NBO) and quantum theory of atoms in molecule (QTAIM) analysis

The values of average natural bond orbital (NBO) analysis of the structures both prior and after H_2 adsorption are given in Table 3. The average NBO charge of all the structures are listed in Table S1 (Supplementary Information). The computed average NBO charges for B, AM/AEM, H_2 adsorbed complexes, and bare B, AM/AEM along with the corresponding number of hydrogen molecules are depicted in Fig. 2. The average charges on the B atom of the bare structure range from − 0.073 to − 0.140 e. However, upon functionalization with AM/AEM atoms, these charges experience a reduction and range from − 0.011 to − 0.085 e. The results show that B atom contains vacant p orbitals and predict that during the adsorption process about 0.006 e–0.669 e NBO charges are transferred from metal atom (AM/AEM) to B atom (− 0.011 e to − 0.085 e). This results exhibit the occurrence of charge transfer from metal atoms to the boron cluster. As a result of the charge transfer taking place between the metal atoms and boron cluster, bonds at B-Li of $B_{20}Li_2$-$6H_2$ complex is altered by 0.232 Å exhibiting the presence of strong interactions prevailing. Similar changes are also observed for Na, K, and alkaline earth metal–interacted H_2 molecules.

With the aid of topological descriptors, the nature of contact between the host clusters and its H_2 interacted complexes is investigated using the quantum theory of atoms in molecules (QTAIM), and the corresponding results are listed in Table 4. The values of electron density (ρ) and Laplacian of electron density ($\nabla^2\rho$) are found to be in the range of 0.0415–0.0211 a.u. and 0.0415–0.0271 a.u. at M-H for all the H_2 adsorbed

Table 3 Average NBO charge of each atoms (e), for $B_{20}AM$ and $B_{20}AEM$ cluster before and after H_2 adsorption

Complexes	Before H_2 adsorption		After H_2 adsorption		
	Q_B	Q_{AM} /Q_{AEM}	Q_B	Q_{AM} /Q_{AEM}	Q_H
$B_{20}Li_2$	−0.074	0.736	−0.011	0.006	0.026
$B_{20}Na_2$	−0.077	0.768	−0.038	0.226	0.020
$B_{20}K_2$	−0.073	0.729	−0.052	0.382	0.019
$B_{20}Ca_2$	−0.119	1.191	−0.085	0.669	0.032
$B_{20}Mg_2$	−0.140	1.098	−0.047	0.233	0.052
$B_{20}Be_2$	−0.097	0.768	−0.063	0.359	0.136

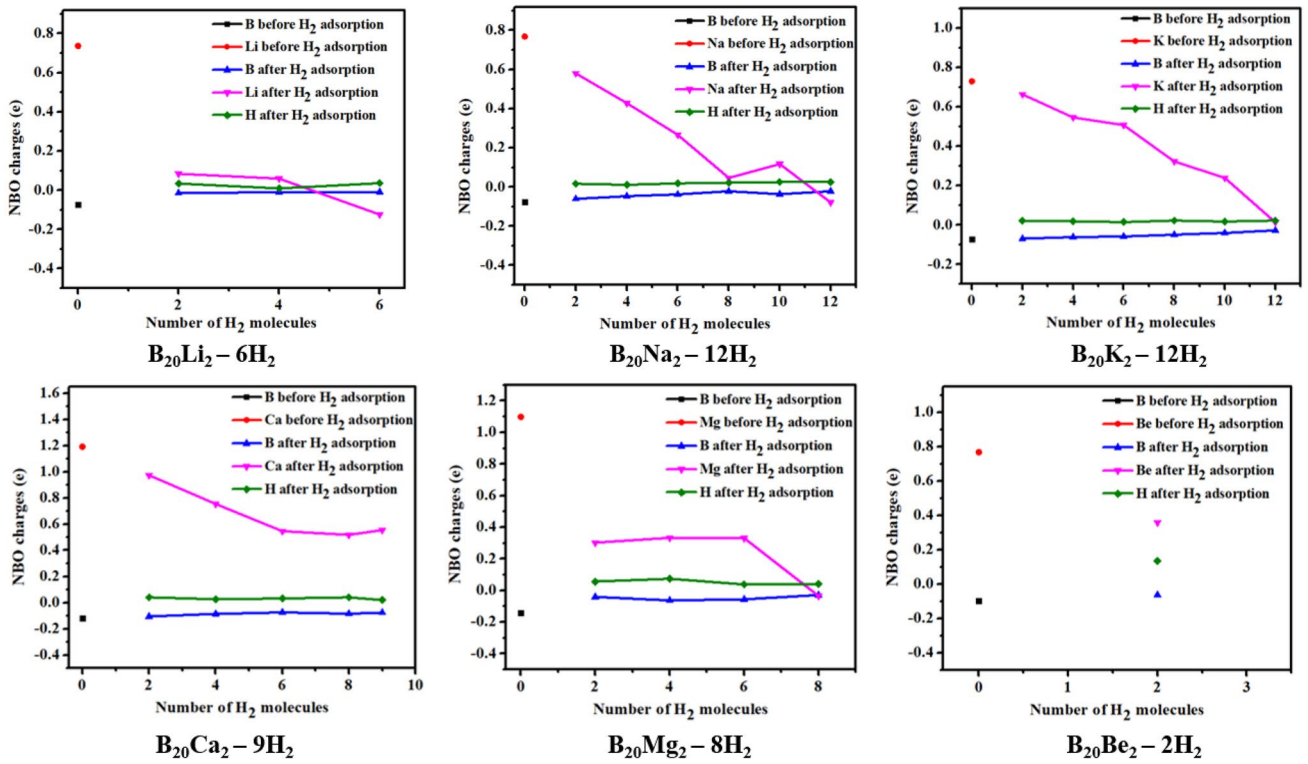

Fig. 2 Average NBO charges before and after hydrogen adsorption of the structures

complexes. The findings show the presence of non-covalent interaction between the metal atoms and the H_2 adsorbed molecule (AM-H/AEM-H). Further, the values for B-AM and B-AEM bond suggest a non-covalent and partially covalent character, while the B-B bond signifies the existence of covalent in nature. Additionally, all the H_2 adsorbed complexes have positive total electron density values ($H(r)$), suggesting that kinetic energy density predominates over potential energy density at BCP (bond critical point).

Non-covalent interaction (NCI)—reduced density gradient (RDG) analysis

The non-covalent interaction (NCI)–reduced density gradient (RDG) analysis of the considered complexes was performed to determine the intramolecular and intermolecular interactions, while also categorizing the types and strengths of these interactions. To precisely illustrate the regions of interaction, we generated plots of the reduced density gradient (RDG) alongside the sign(λ_2)$\rho(r)$. The sign(λ_2)$\rho(r)$ value was utilized to distinguish between strong and weak non-covalent interactions. The NCI scatter plots and corresponding isosurfaces for the complexes are visualized in Fig. 3. The scatter plot of sign(λ_2)$\rho(r)$ versus RDG covers a range from – 0.05 to 0.05 a.u. The sign(λ_2)$\rho(r)$ values are positioned on the X-axis, while the RDG values are presented on the vertical axis. The NCI analysis is elucidated using a color scale: red signifies areas with repulsive interactions due to steric effects; blue-colored regions denote interactions arising from hydrogen bonds. Additionally, green regions indicate van der Waals (Vdw) interactions. In the preceding section, quantum theory of atoms in molecules (QTAIM) analysis predicted the presence of non-covalent interactions between hydrogen molecules and metal atoms, as well as between boron and metal atoms within the complexes. Similarly, in Fig. 3, the green regions are evident around the hydrogen molecules and the metal atoms, as well as between boron and metal atoms, which can be attributed to van der Waals interactions. Additionally, red regions appear along the B-B and B-AEM bonds of the complexes, indicating repulsive interactions in those regions.

Adsorption energy

The average adsorption energy (E_{ads}) and wt% of the system calculated at the same level of theory are shown in Table 5. Furthermore, the values are compared with those of previously documented boron-based 2D nanostructures. The values of E_{ads} are determined to fall between 0.094 and 0.503 eV/H_2. The results show that E_{ads} values are positive for the entire H_2 adsorbed host cluster suggesting that the H_2 adsorption mechanism is exothermic in nature. The gravimetric densities of all

Table 4 The topological parameters (in a.u.) of the structures obtained at ωB97XD/6–311 + + G(d,p) level of theory

Complexes	BCP	ρ	$\nabla^2\rho$	$G(r)$	$V(r)$	$H(r)$
$B_{20}Li_2$	B-B	0.1531	−0.2678	0.0484	−0.1534	−0.1692
	B-Li	0.0177	0.0779	0.0179	−0.0160	0.0018
$B_{20}Li_2$–$6H_2$	B-B	0.1492	−0.2565	0.0463	−0.1567	−0.1104
	B-Li	0.0152	0.0700	0.0155	−0.0135	0.0020
	Li–H	0.0068	0.0415	0.0082	−0.0060	0.0022
	H–H	0.2589	−1.0401	0.0005	−0.2616	−0.2611
$B_{20}Na_2$	B-B	0.1515	−0.2703	0.0456	−0.1587	−0.1131
	B-Na	0.0115	0.0485	0.0104	−0.0087	0.0017
$B_{20}Na_2$–$12H_2$	B-B	0.1272	−0.2313	0.0379	−0.1336	−0.0957
	B-Na	0.0089	0.0390	0.0081	−0.0064	0.0017
	Na–H	0.0052	0.0271	0.0052	−0.0035	0.0016
	H–H	0.0029	0.0077	0.0015	−0.0011	0.0004
$B_{20}K_2$	B-B	0.1436	−0.2095	0.0474	−0.1471	−0.1634
	B-K	0.0115	0.0377	0.0082	−0.0070	0.0012
$B_{20}K_2$–$12H_2$	B-B	0.1447	−0.2437	0.0424	−0.1458	−0.1034
	B-K	0.0080	0.0229	0.0049	−0.0041	0.0009
	K-H	0.0049	0.0211	0.0039	−0.0026	0.0013
	H–H	0.2590	−1.0502	0.0003	−0.2620	−0.2617
$B_{20}Ca_2$	B-B	0.1475	−0.2437	0.0471	−0.1551	−0.1080
	B-Ca	0.1070	0.0863	0.0232	−0.0249	−0.0002
$B_{20}Ca_2$–$9H_2$	B-B	0.1463	−0.2346	0.0486	−0.1558	−0.1836
	B-Ca	0.0245	0.0729	0.0188	−0.0194	−0.0006
	Ca-H	0.0099	0.0369	0.0077	−0.0061	0.0016
	H–H	0.2562	−1.0262	0.0009	−0.2584	−0.2575
$B_{20}Mg_2$	B-B	0.1392	−0.2208	0.0455	−0.1378	−0.1012
	B-Mg	0.0362	0.1040	0.0300	−0.0340	−0.0040
$B_{20}Mg_2$–$8H_2$	B-B	0.1453	−0.2372	0.0449	−0.1491	−0.1845
	B-Mg	0.0341	0.1063	0.0296	−0.0326	−0.0030
	Mg-H	0.0090	0.0305	0.0068	−0.0060	0.0008
	H–H	0.2566	−1.0288	0.0008	−0.1550	−0.2580
$B_{20}Be_2$	B-B	0.1471	−0.2441	0.0473	−0.1557	−0.1084
	B-Be	0.0590	0.1402	0.0567	−0.0784	−0.0217
$B_{20}Be_2$–$2H_2$	B-B	0.1429	−0.2388	0.0416	−0.1429	−0.1013
	B-Be	0.0597	0.1482	0.0587	−0.0802	−0.0216
	Be-H	0.0382	0.2258	0.0560	−0.0556	0.0004
	H–H	0.2468	−0.9386	0.0046	−0.2439	−0.2392

the complexes are determined to be in the range of 1.66–8.33 wt % which is well in agreement with the US Department of Energy (DOE) predicted value (5.5 wt% by 2025). However, in the present work $B_{20}Li_2$–$6H_2$ and $B_{20}Be_2$–$2H_2$ complex gravimetric densities are less than the US DOE targeted value. Table 5 provides additional insights, revealing that the B_{20} nanostructures decorated with alkali and alkaline earth metals exhibit higher gravimetric capacities than those reported in previous literature, with the exception of the Li and Be decorated structures. The structure $B_{20}Na_2$ can store up to $12H_2$ molecules, resulting in a relatively high gravimetric density of 8.33 wt% and the complex suggests that it can be the most prospective candidate for hydrogen storage.

Molecular dynamics simulations

To investigate the adsorption and desorption processes at room temperature, we performed atom-centered density matrix propagation (ADMP)–molecular dynamics (MD) simulation of all the complexes. The simulations were carried out for duration of 200 fs. The trajectories of the complexes are visualized in Fig. 4, while snapshots captured at various time intervals are provided in Fig. S1 (Supplementary Information). The observations of the results revealed that within specific time intervals of 30 fs, 20 fs, 20 fs, 30 fs, 30 fs, and 50 fs, the first H_2 molecules began to move away from the $B_{20}Li_2$–$6H_2$,

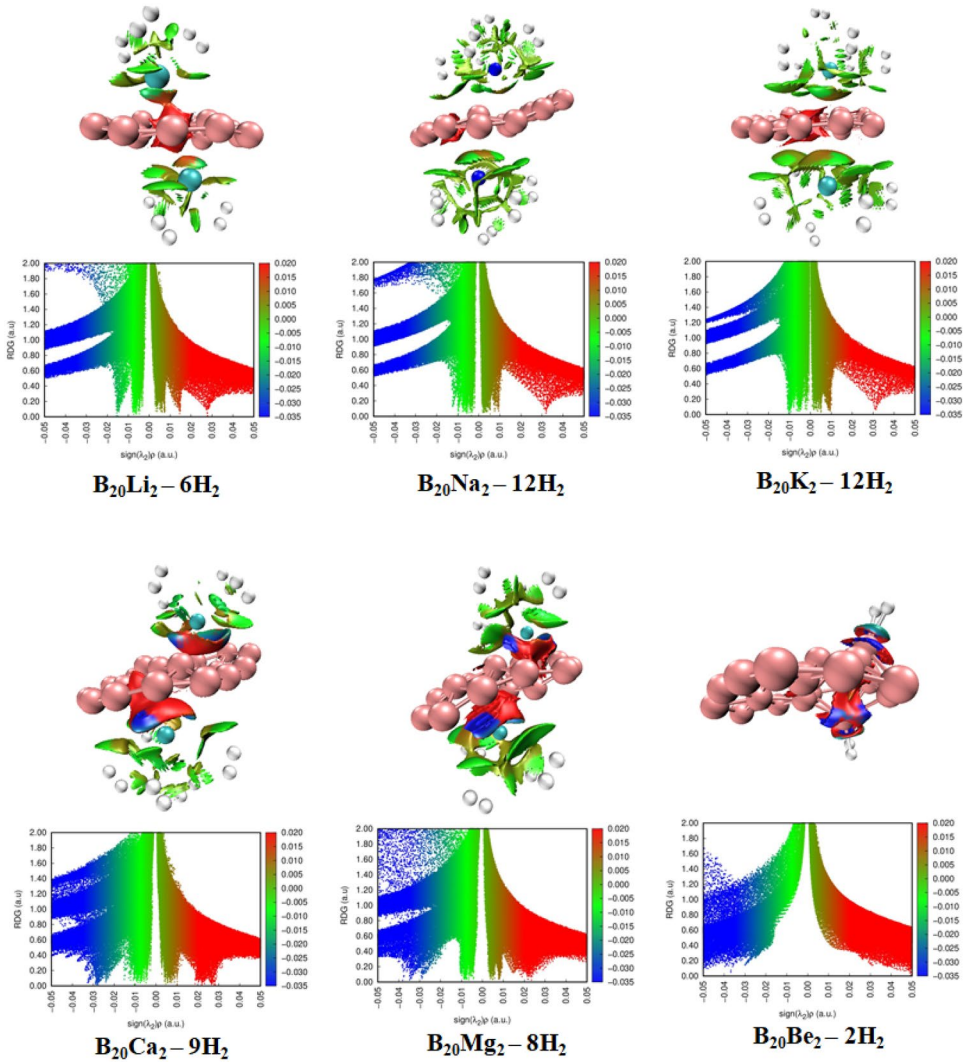

Fig. 3 The plot of sign(λ_2)ρ(r) (a.u.) and reduced density gradient (RDG) for all the complexes

Table 5 Average adsorption energy per H_2 molecule (E_{ads}) and gravimetric density

Complexes	E_{ads} (eV)	wt%	Literature	
			Structure	wt%
$B_{20}Li_2$–$6H_2$	0.181	4.91	$B_{40}Li_6$-$18H_2$ [32]	7.10
$B_{20}Na_2$–$12H_2$	0.127	8.33	$B_{36}Na_2$-$10H_2$ [23]	4.40
$B_{20}K_2$–$12H_2$	0.094	7.51	$B_{28}K_3$-$14H_2$ [40]	6.30
$B_{20}Ca_2$–$9H_2$	0.188	5.70	$B_{36}Ca_2$-$12H_2$ [26]	4.97
$B_{20}Mg_2$–$8H_2$	0.141	5.67	B_9Mg_2-$4H_2$ [41]	5.20
$B_{20}Be_2$–$2H_2$	0.503	1.66	B_8Be_2-$7H_2$ [42]	21.1

$B_{20}Na_2$–$12H_2$, $B_{20}K_2$–$12H_2$, $B_{20}Ca_2$–$9H_2$, $B_{20}Mg_2$–$8H_2$, and $B_{20}Be_2$–$2H_2$ complexes, respectively. Through the MD simulations, we found that even after 200 fs, $2H_2$, $5H_2$, $3H_2$, $1H_2$, $1H_2$, and $2H_2$ molecules remained bound to the $B_{20}Li_2$, $B_{20}Na_2$, $B_{20}K_2$, $B_{20}Ca_2$, $B_{20}Mg_2$, and $B_{20}Be_2$ clusters, respectively. Notably, there were minimal changes in the geometrical characteristics of the clusters even after the desorption process. This suggests that these clusters hold promising potential for reversible H_2 storage.

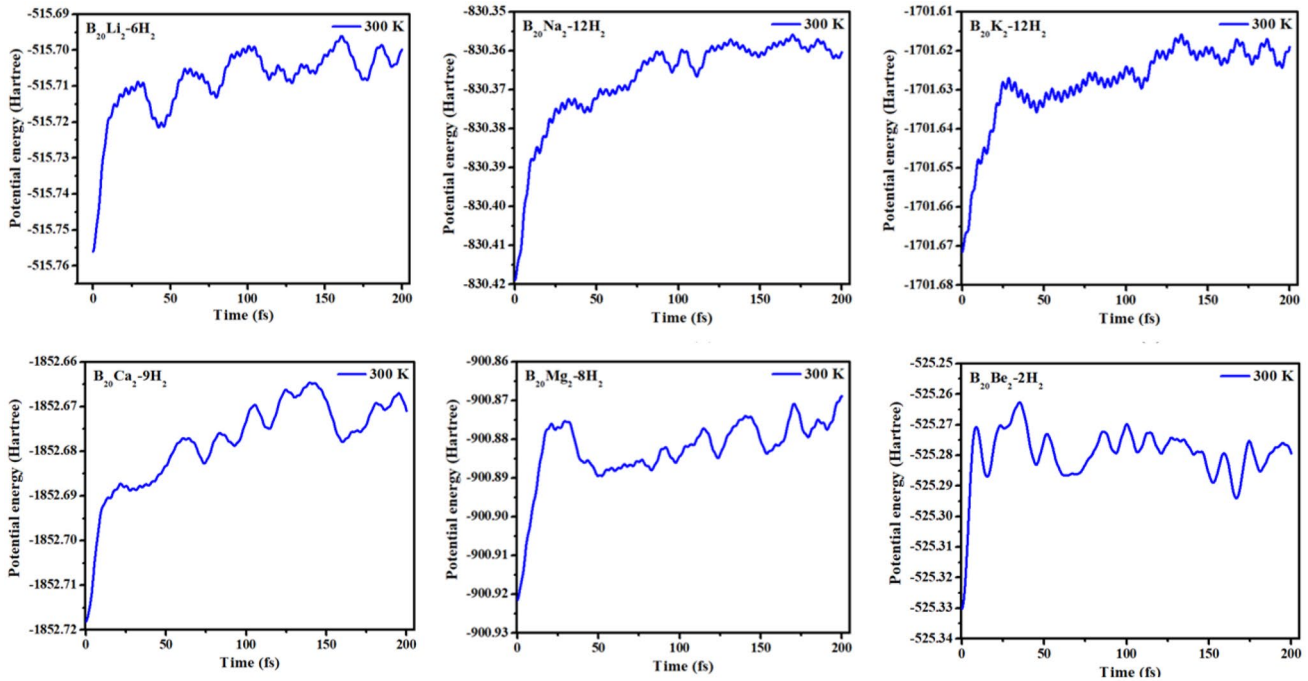

Fig. 4 The ADMP trajectories of the structures at room temperature

Conclusions

The ability of B_{20} cluster decorated with alkali (AM = Li, Na, and K) and alkaline earth metals (AEM = Ca, Mg, and Be) to capture hydrogen atoms is explored using density functional theory (DFT) calculations. The electronic properties explain the stability of the structures which are supported by their enhanced chemical hardness and decreased electrophilicity index. The global reactivity values affirm that the structure remains stable even after the adsorption of H_2 molecules. Topological parameters revealed that the interaction between bare structures and metal atoms is of closed shell type. Furthermore, a maximum of $6H_2$ molecules can be attached by each Na and K atoms of the $B_{20}Na_2$ and $B_{20}K_2$ complexes with a gravimetric density of 8.33 and 7.51 wt%, respectively. Based on our results we suggest that AM and AEM decorated B_{20} cluster could definitely be a promising material for hydrogen storage applications. Molecular dynamics simulations using ADMP were conducted under room temperature. The findings revealed that the $B_{20}Li_2$, $B_{20}Na_2$, $B_{20}K_2$, $B_{20}Ca_2$, $B_{20}Mg_2$, and $B_{20}Be_2$ clusters maintained a binding of up to $2H_2$, $5H_2$, $3H_2$, $1H_2$, $1H_2$, and $2H_2$ molecules, respectively, attached to their respective metal centers.

Supplementary Information The online version contains supplementary material available at https://doi.org/10.1007/s11224-023-02226-9.

Author contribution PDD and PMPS: conceptualization, investigation, data curation, formal analysis, methodology, visualization, and roles/writing—original draft. PG and AA: formal analysis, software, resources, supervision, validation, and writing—review and editing. All authors read and approved the final manuscript.

Availability of data and materials The authors confirm that the data supporting the findings of this study are available within the article and as supplemetary material.

Code availability Not applicable.

Declarations

Conflict of interest The authors declare no competing interests.

References

1. Isidro-Ortega FJ, Pacheco-Sánchez JH, González-Ruíz A, Alejo R (2020) DFT study of hydrogen storage on the metallic decoration of boron substitution on zeolite templated carbon vacancy. Int J Hydrogen Energy 45:19505–19515. https://doi.org/10.1016/j.ijhydene.2020.05.017
2. Prasetyo N, Pambudi FI (2021) Toward hydrogen storage material in fluorinated zirconium metal-organic framework (MOF-801): a periodic density functional theory (DFT) study of fluorination and adsorption. Int J Hydrogen Energy 46:4222–4228. https://doi.org/10.1016/j.ijhydene.2020.10.222
3. Ray SS, Sahoo RK, Sahu S (2022) Reversible hydrogen storage capacity of vanadium decorated small boron clusters (B_nV_2, n = 6–10): a dispersion corrected density functional study. Comput Theor Chem 1217:113899. https://doi.org/10.1016/j.comptc.2022.113899
4. Jena P (2011) Materials for hydrogen storage: past, present, and future. J Phys Chem Lett 2:206–211. https://doi.org/10.1021/jz1015372

5. Hydrogen Storage. http://energy.gov/eere/fuelcells/hydrogen-storage
6. Kassaoui EL, M, Loulidi M, Benyoussef A et al (2023) Tuning hydrogen storage properties of Li- and Na-decorated 3D carbon-honeycomb through a physisorption process. Energy Fuels 37:8689–8698. https://doi.org/10.1021/ACS.ENERGYFUELS.3C00708/SUPPL_FILE/EF3C00708_SI_001.PDF
7. Kassaoui EL, M, Houmad M, Lakhal M et al (2021) Hydrogen storage in lithium, sodium and magnesium-decorated on tetragonal silicon carbide. Int J Hydrogen Energy 46:24190–24201. https://doi.org/10.1016/J.IJHYDENE.2021.04.183
8. Mahamiya V, Shukla A, Chakraborty B (2022) Scandium decorated C_{24} fullerene as high capacity reversible hydrogen storage material: insights from density functional theory simulations. Appl Surf Sci 573:151389. https://doi.org/10.1016/J.APSUSC.2021.151389
9. Mahamiya V, Shukla A, Chakraborty B (2022) Exploring yttrium doped C_{24} fullerene as a high-capacity reversible hydrogen storage material: DFT investigations. J Alloys Compd 897. https://doi.org/10.1016/j.jallcom.2021.162797
10. EL Kassaoui M, Mansouri Z, Al-Shami A et al (2022) Design of metal-decorated beryllium carbide (Be_2C) as a high-capacity hydrogen storage material with strong adsorption characteristics. Appl Surf Sci 589:152960. https://doi.org/10.1016/J.APSUSC.2022.152960
11. Kassaoui EL, M, Lakhal M, Benyoussef A et al (2022) Improvement of the hydrogen storage performance of t-graphene-like two-dimensional boron nitride upon selected lithium decoration. Phys Chem Chem Phys 24:15048–15059. https://doi.org/10.1039/D2CP00480A
12. Bäoyäukata M, ÄozdoGan C, Gäuvenc ZB (2008) Hydrogen hosting of nano scale boron clusters. Rom J Inf Sci Technol 11:59–70
13. Tang C, Wang Z, Zhang X, Wen N (2016) The hydrogen storage properties of Na decorated small boron cluster B_6Na_8. Chem Phys Lett 661:161–167. https://doi.org/10.1016/j.cplett.2016.08.064
14. Song N, Lv J, Wang Y (2013) B_{24} cluster as promising material for lithium storage and hydrogen storage applications. Comput Mater Sci 77:31–34. https://doi.org/10.1016/j.commatsci.2013.03.043
15. Dong H, Hou T, Lee ST, Li Y (2015) New Ti-decorated B_{40} fullerene as a promising hydrogen storage material. Sci Rep 5:1–8. https://doi.org/10.1038/srep09952
16. Dewangan J, Mahamiya V, Shukla A, Chakraborty B (2022) Lithium decorated Ψ-graphene as a potential hydrogen storage material: density functional theory investigations. Int J Hydrogen Energy. https://doi.org/10.1016/J.IJHYDENE.2022.10.142
17. Mahamiya V, Shukla A, Chakraborty B (2022) Potential reversible hydrogen storage in Li-decorated carbon allotrope PAI-Graphene: a first-principles study. Int J Hydrogen Energy. https://doi.org/10.1016/J.IJHYDENE.2022.11.016
18. Chkhartishvili L (2022) Relative stability of boron planar clusters in diatomic molecular model. Molecules 27. https://doi.org/10.3390/molecules27051469
19. Atiş M, Zdoan C, Güvenç ZB (2009) Density functional study of physical and chemical properties of nano size boron clusters: B_n (n=13-20). Chinese J Chem Phys 22:380–388. https://doi.org/10.1088/1674-0068/22/04/380-388
20. Lu QL, Huang SG, De LY et al (2015) Alkali and alkaline-earth atom-decorated B38 fullerenes and their potential for hydrogen storage. Int J Hydrogen Energy 40:13022–13028. https://doi.org/10.1016/j.ijhydene.2015.08.008
21. Haldar S, Mukherjee S, Singh CV (2018) Hydrogen storage in Li, Na and Ca decorated and defective borophene: a first principles study. RSC Adv 8:20748–20757. https://doi.org/10.1039/C7RA12512G
22. Mahamiya V, Shukla A, Chakraborty B (2022) Ultrahigh reversible hydrogen storage in K and Ca decorated 4–6-8 biphenylene sheet. Int J Hydrogen Energy 47:41833–41847. https://doi.org/10.1016/J.IJHYDENE.2022.01.216
23. Ye XJ, Teng ZW, Le YX, Liu CS (2018) Na-coated hexagonal B_{36} as superior hydrogen storage materials. J Saudi Chem Soc 22:84–89. https://doi.org/10.1016/j.jscs.2017.07.006
24. Yuanchang L, Gang Z, Jia L et al (2008) Alkali-metal-doped B_{80} as high-capacity hydrogen storage media. J Phys Chem C 112:19268–19271. https://doi.org/10.1021/jp807156g
25. Mao J, Guo P, Zhang T et al (2020) A first-principle study on hydrogen storage of metal atoms (M = Li, Ca, Sc, and Ti) coated B_{40} fullerene composites. Comput Theor Chem 1181:112823. https://doi.org/10.1016/j.comptc.2020.112823
26. Liu P, Liu F, Peng Y et al (2019) A DFT study of hydrogen adsorption on Ca decorated hexagonal B_{36} with van der Waals corrections. Phys E Low-Dimensional Syst Nanostructures 114:113576. https://doi.org/10.1016/j.physe.2019.113576
27. Wang J, Du Y, Sun L (2016) Ca-decorated novel boron sheet: a potential hydrogen storage medium. Int J Hydrogen Energy 41:5276–5283. https://doi.org/10.1016/j.ijhydene.2016.01.039
28. Kiran B, Bulusu S, Zhai HJ et al (2005) Planar-to-tubular structural transition in boron clusters: B_{20} as the embryo of single-walled boron nanotubes. Proc Natl Acad Sci U S A 102:961–964. https://doi.org/10.1073/pnas.0408132102
29. An W, Bulusu S, Gao Y, Zeng XC (2006) Relative stability of planar versus double-ring tubular isomers of neutral and anionic boron cluster B_{20} and B_{20}^-. J Chem Phys 124. https://doi.org/10.1063/1.2187003
30. Lu QL, Luo QQ, De LY, Huang SG (2017) Planarization of B_{20} clusters by Si and C atom substitution. Phys Chem Chem Phys 19:28434–28438. https://doi.org/10.1039/c7cp05610a
31. Guo C, Wang C (2018) Computational investigation of hydrogen storage on $B_6Ti_3^+$. Int J Hydrogen Energy 43:1658–1666. https://doi.org/10.1016/j.ijhydene.2017.11.161
32. Bai H, Bai B, Zhang L et al (2016) Lithium-decorated borospherene B_{40}: a promising hydrogen storage medium. Sci Rep 6:1–10. https://doi.org/10.1038/srep35518
33. Liu P, Zhang Y, Liu F (2022) Study of the reversible hydrogen storage performance of Ti-decorated hexagonal B_{36} by DFT calculations with van der Waals corrections. Int J Hydrogen Energy 47:25696–25703. https://doi.org/10.1016/j.ijhydene.2022.05.304
34. Da CJ, Head-Gordon M (2008) Long-range corrected hybrid density functionals with damped atom-atom dispersion corrections. Phys Chem Chem Phys 10:6615–6620. https://doi.org/10.1039/b810189b
35. Krishnan R, Binkley JS, Seeger R, Pople JA (1980) Self-consistent molecular orbital methods. XX. A basis set for correlated wave functions. J Chem Phys 72:650–654. https://doi.org/10.1063/1.438955
36. Lu T, Chen F (2012) Multiwfn: a multifunctional wavefunction analyzer. J Comput Chem 33:580–592. https://doi.org/10.1002/jcc.22885
37. Koopmans T (1934) On the assignment of wave functions and eigenvalues to the individual electrons of an atom. Physica 1:104–113. https://doi.org/10.1016/S0031-8914(34)90011-2
38. Frisch MJ, Trucks GW, Schlegel HB, Scuseria GE, Robb MA, Cheeseman JR, Scalmani G, Barone V, Mennucci B, Petersson GA, Nakatsuji H, Caricato M, Li X, Hratchian HP, Izmaylov AF, Bloino J, Zheng G, Sonnenberg JL, Hada M, Ehara M, Toyota K, Fukuda R, Hasegawa J, Ishida M, Nakajima T et al (2009) Gaussian 09, Revision B.01
39. Chemcraft - graphical software for visualization of quantum chemistry computations. https://www.chemcraftprog.com
40. Si L, Tang C (2017) The reversible hydrogen storage abilities of metal Na (Li, K, Ca, Mg, Sc, Ti, Y) decorated all-boron cage B_{28}. Int J Hydrogen Energy 42:16611–16619. https://doi.org/10.1016/j.ijhydene.2017.05.181
41. Kumar A, Vyas N, Ojha AK (2020) Hydrogen storage in magnesium decorated boron clusters (Mg_2B_n, n = 4–14): a density functional

theory study. Int J Hydrogen Energy 45:12961–12971. https://doi.org/10.1016/j.ijhydene.2020.03.018
42. Wang YJ, Xu L, Qiao LH et al (2020) Ultra-high capacity hydrogen storage of B_6Be_2 and B_8Be_2 clusters. Int J Hydrogen Energy 45:12932–12939. https://doi.org/10.1016/j.ijhydene.2020.02.209